In addition to the step responses, continuous driving characteristics of the microplatforms with 2×2 and 2×3 PMs were studied. Fig. 9(a) shows the displacement of the microplatform with 2×2 PMs with a driving current of 0.15 A. The continuous step motions are based on the step response as shown in Fig. 8(a). The final displacement after the three step motions is 5.2 mm, which is equivalent to one and a half coils. Fig. 9(b) shows the continuous displacement of the microplatform with 2×3 PMs. The step motion for the microplatform with 2×3 PMs is similar to that for the microplatform with 2×2 PMs.

B. Evaluations

Final values (displacements) are defined by using the experimental results shown in Fig. 8. Fig. 10 shows the experimental result for the microplatforms with 2×2 PMs (filled circles) and 2×3 PMs (open circles). Each final value (displacement) increases with increasing current in the range up to 0.3 A. The maximum displacements are about 1.38 and 1.81 mm.

Final displacements of the microplatforms with 2×2 PMs and 2×3 PMs were measured with some loads of 0.05, 0.10, 0.20, and 0.3 g. The results for the microplatforms with 2×2 PMs and 2×3 PMs are shown in Fig. 11(a) and (b), respectively. From Fig. 11, the final displacement for each load increases with increasing driving current. The displacement also increases with decreasing carrying loads. The final displacements in Fig. 11 are smaller than the displacements without loads in Fig. 10. In general, the displacements in Fig. 11(b) are larger than those in Fig. 11(a).

IV. Conclusion

In this study, the magnetically driven linear microactuator using microsystem fabrication techniques is successfully developed. From the results, the driving method is found to be available for driving the microplatform. The final values of the step responses depend on the driving currents. From the study on carrying capacity, it is found that the microplatform carries about the same load as itself. The microplatform shows the continuous motion according to the computer signals. As a result, the microactuator mentioned previously is found to be useful for some kinds of applications such as microconveyer.

References

[1] K. S. J. Pister, R. S. Fearing, and R. T. Howe, "A planar air levitated electrostatic actuator system," in *Proc. IEEE MEMS Workshop*, Napa Valley, CA, Feb. 1990, pp. 67–71.

[2] H. Guckel, K. J. Skrobis, T. R. Christenson, J. Klein, S. Ham, B. Choi, E. G. Lovell, and T. W. Champman, "Fabrication and testing of the planar magnetic micromotor," *J. Micromech. Microeng.*, vol. 1, no. 4, pp. 135–138, Sep. 1991.

[3] M. Komori and T. Yamane, "Magnetically levitated micro PM motors by two types of active magnetic bearings," *IEEE/ASME Trans. Mechatronics*, vol. 6, no. 1, pp. 43–49, 2001.

[4] B. Wagner, M. Kreutzer, and W. Benecke, "Permanent magnet micromotors on silicon substrates," *J. Microelectromech. Syst.*, vol. 2, no. 1, pp. 23–29, Mar. 1993.

[5] L. K. Lagorce, O. Brand, and M. G. Allen, "Magnetic microactuators based on polymer magnets," *J. Microelectromech. Syst.*, vol. 8, no. 1, pp. 2–9, Mar. 1999.

Uncoupling Micromachined-Based Piezoelectric Accelerometer Performance From a Sensor Structure Transfer Function

Yu-Hsiang Hsu, Chih-Kung Lee, Long-Sun Huang, Chih-Cheng Chu, and Ta-Shun Chu

***Abstract*—A smart structure technology for autonomous gain and phase tailoring was adapted to develop a new accelerometer that possesses both an excellent low-frequency response and a high operational bandwidth. The freedom associated with the uncoupling of the gain and phase tailoring to an accelerometer-based structure transfer function can be shown to vastly expand the performance area of traditional accelerometers. We used free-fall detection to demonstrate this newly found capability with its wide applicability to portable devices and which is perceived as extremely difficult to pursue for magnetic disk drives. A micromachined accelerometer was developed to demonstrate the expanded applicability of this innovative concept that integrates smart structure technology to accelerometer design. Both theoretical derivations and experimental verification of this new class of accelerometers are detailed in this paper.**

***Index Terms*—Free-fall sensors, microsensors, point sensors, smart structures.**

I. Introduction

Because the performance of an accelerometer is most prominently demonstrated by its frequency response, the frequency and the damping factor associated with the first resonant mode becomes the primary design concern whenever a new potential accelerometer is developed. In fact, this implicit rule of thumb effectively limits an accelerometer bandwidth to 1/10 to 1/5 of its first resonant frequency such that the achieved linearity and accuracy will be better than 5–10% [1]. Because accelerometer performance is so tightly linked to the base structure, the operational bandwidth and the sensitivity required almost immediately determine the size of the accelerometer. In this article we incorporate smart structure technology developed over the past two decades [2] into an accelerometer design. This concept provides us with a method to vastly expand the design freedom of accelerometers, which was first reported by Hsu and Lee in 2002 [3]. At that time, to clearly illustrate the impact of this series of sensors, the concepts of point-distributed sensors (named PoD sensors) and APROPOS devices (acronym for autonomous phase-gain rotation/linear piezoelectric optimal sensing) were described [3]. This study reported that the usable bandwidth of this newly developed accelerometer can be enhanced by incorporating an APROPOS device onto a PoD sensor, as gain and phase tailoring are autonomous [3]. To verify the sensitivity and applicability of this newly invented piezoelectric accelerometer as a micromachine-based device and to explore application areas not attainable by previous accelerometers, a free-fall motion was chosen as the metrology target in this article [4]. It is worth noting that free-fall sensing has been deemed an important research and development target of the magnetic

Manuscript received October 15, 2003; revised July 12, 2004 and January 17, 2005. This work was supported by the National Science Council of Taiwan, R.O.C., under Grant NSC 85-2622-E-002-017R, Grant NSC 86-2622-E-002-023R, Grant NSC 88-2218-E-002-005, and Grant NSC 88-2622-E-002-001. Recommended by Technical Editor J. von Amerongen.

Y.-H. Hsu was with the Institute of Applied Mechanics, National Taiwan University, Taipei, Taiwan, R.O.C. He is now with the University of California, Irvine, CA 92697 USA (e-mail: yuhsiang@uci.edu).

C.-K. Lee, L.-S. Huang, C.-C. Chu, and T.-S. Chu are with the Institute of Applied Mechanics, National Taiwan University, Taipei, Taiwan, R.O.C. (e-mail: cklee@ntu.edu.tw; lshuang@mems.iam.ntu.edu.tw; ccchu@mems.iam.ntu.edu.tw; tschu@mems.iam.ntu.edu.tw).

Digital Object Identifier 10.1109/TMECH.2005.848301

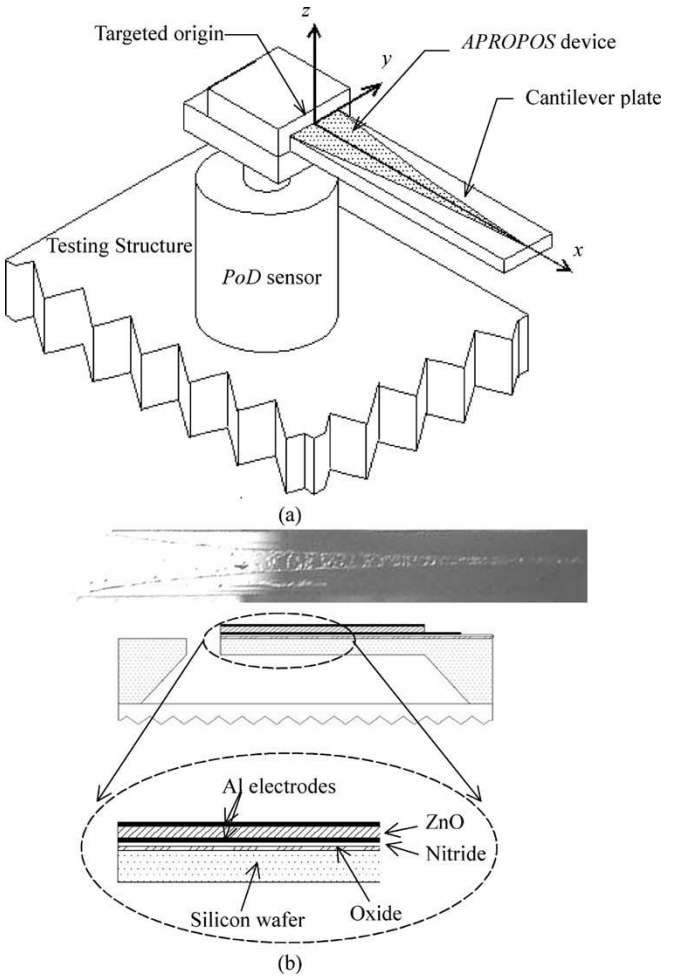

Fig. 1. (a) Schematic of a PoD sensor designed by an APROPOS device. (b) Top view of a micromachine-based PoD sensor design incorporating an APROPOS device and its side view of the micromachine-based PoD sensor, where Al electrodes are 0.2 μm thick, silicon wafer is 500 μm thick, ZnO is 1.0 μm thick, nitride is 0.15 μm thick, and oxide is 0.1 μm thick.

disk drive industry for the past 25 years because of the rapid advancement of portable devices [4]. Nevertheless, the difficulty of detecting the start of a free fall has hindered the implementation of this line of technology [5].

II. Concepts of PoD Sensors

Fig. 1(a) shows the chosen schematic of the PoD sensor in this article where a one-dimensional cantilever plate is the flexible structure and where the structure serves as the sensor structure of the PoD sensor to measure the targeted vibration source from the testing structure. Because the APROPOS device can offer spatial weighting in a spatial domain by utilizing its distributed sensor attached onto a small size flexible structure [3], a no-phase delay low-pass filter can be embedded in the sensor transfer function of the PoD sensor shown in Fig. 1(a). Thus, this PoD sensor acts as a point sensor while having the advantage of possessing a good low-frequency sensitivity in addition to a wide usable bandwidth derived from the distributed sensor technology. Because the frequency range of the flexible structure implemented by a micromachine process [6] is in the range of kilohertz to several kilohertz, a micromachine-based accelerometer serves as the best matching platform for implementing a PoD sensor. In this article, a micromachine-based PoD sensor designed by an APROPOS device will be demonstrated to clearly show the importance of this newly invented accelerometer. The basic theory and design flow of APROPOS devices by Hsu and Lee can be found in a separate paper [3] and will not be repeated in this article.

III. Concept and Implementation of APROPOS Devices

The basic geometry of distributed sensor is similar to the one-dimensional plate shown in Fig. 1(a), where various distributed sensor designs are attached to one-dimensional flexible structures [2]. A spatial weighting function is applied to the y axis to modulate the structure strain in the x direction, that is, the measured structure characteristic of this distributed sensor is the combination of an overall monitored structure characteristic and additional filtering effect in a spatial domain. The design concept of the APROPOS device form the bases for us (1) to express the bending displacement as four wave modes (e.g., propagation waves e^{jkx} and e^{-jkx} and evanescent waves e^{-kx} and e^{-kx}), (2) to use the method of image mathematical tool to expand these four wave modes into an infinite domain (i.e., allow the four discontinuous waves to propagate in an imaginary infinite domain), (3) to apply zero weighting to the discontinuous waves by the effective surface electrode which occur at the boundaries, and (4) to merge each of the two waves of the propagating waves and evanescent waves by using a symmetric effective surface electrode $R_e(x)$ with respect to its origin. Thus the sensor equation can be written as [3]

$$q(k) = -z_k d_{31} k^2 e^{-j\omega t}\left[-(w_{lp}+w_{rp})\int_{-\infty}^{\infty} R_e(x)e^{-jkx}dx + (w_{le}+w_{re})\int_{-\infty}^{\infty} R_e(x)e^{-kx}dx\right]. \quad (1)$$

By considering each wave mode as a two-sided Laplace transform, a no-phase delay low-pass filter was proved possible to be implemented in a spatial domain with a proper surface electrode $R(x)$ [3]. This is the fundamental reason why an APROPOS device can perform autonomous gain and phase tailoring. It can be seen from (1) that this spatial filtering effect is executed externally to the original structure characteristics, which is the local strain of the origin. This point is known as the targeted origin $w''(x,t) = -k^2 e^{-j\omega t}[-(w_{lp}+w_{rp}) + (w_{le}+w_{re})]$. Thus, the transfer function of an APROPOS device is the superposition of the characteristics of the structure, the local characteristics of the targeted origin, and the spatial filtering effect.

Because external vibrations are transmitted to the accelerometer from the fixed end, the targeted origin was placed exactly at this fixed end [Fig. 1(a)] to ensure the accelerometer output equaled the no-phase delay low-pass filter multiplied by the sensor structure response, as measured with the fixed end as the sensing point. As Hsu and Lee [3] previously reported that an APROPOS device with a targeted origin placed at a fixed-end has an odd-function effective surface electrode in an infinite domain, the integration by parts when applied to the sensor equation in (1) can be written as

$$\begin{aligned} q_k(t) &= -z_k e_{31}\left[\left(R_e'(x)\frac{\partial^2 w}{\partial x^2}\right)\Big|_{-\infty}^{\infty} - \int_{-\infty}^{\infty} R_e(x)\frac{\partial^3 w}{\partial x^3}dx\right] \\ &= z_k e_{31} e^{j\omega t} k^2\left[(-jkw_{lp}+jkw_{rp})\int_{-\infty}^{\infty} R_e(x)e^{-jkx}dx + (kw_{le}-kw_{re})\int_{-\infty}^{\infty} R_e(x)e^{-kx}dx\right] \end{aligned} \quad (2)$$

where the spatial weighting is zero in an infinite domain. Note that the equivalent effective surface electrode $R_e(x)$ of this odd-function

APROPOS device is an even function in (2), that is, $R_e(x) = R'(x)$. This equivalent effective surface electrode $R_e(x)$ has an mathematical form identical with the one in (1). That is, this odd-function APROPOS device offers a no-phase delay filtering effect to the shear force of the targeted origin in an infinite domain.

Following the previously suggested design of Hsu and Lee [3], the effective surface electrode was chosen as

$$R(x) = e^{-\alpha|x|} - c[\sin(\beta x)] \tag{3}$$

where α is a chosen corner wavenumber, β is a chosen wavenumber slightly smaller then the inverse of the length of the one-dimensional plate, and c is a constant to make the weighting at the free end to be zero. By substituting this effective surface electrode into (2) and transfer into a frequency domain [3], the sensor equation becomes

$$q(k) = z_k d_{31} w'''(x = 0, t) \frac{1}{\bar{\alpha} + \omega} \tag{4}$$

where $\bar{\alpha}$ is the transformed corner frequency of the designed corner wavenumber α [3]. It is clear from (4) that this APROPOS device measures the local shear force at the fixed end with a -20 dB/decade no-phase delay low-pass filter in a frequency domain. As this "one-dimensional structure" serves as a sensor structure [Fig. 1(a)], it becomes a "point sensor" having a no-phase delay filtering effect that measures the exiting source from the fixed end. This method provides us with an opportunity to set the corner frequency of the low-pass filter at a very low wave number; e.g., low enough to filter out the influence of the first sensor structure mode.

IV. Miniature Free-Fall Sensors

In 1996, Lee *et al*. [5] experimentally verified that at the moment of a free-fall motion, the acceleration changes from zero to one gravity g instantly. A free-fall sensor to measure the time history of a free-fall motion was first implemented by Hsu and Lee in 2001 [4]. The main idea behind free-fall sensing lies in the fact that an acceleration change is a kind of force response that can be measured by a mechanical structure. Based on the experimental results of Hsu and Lee [4], the frequency range of the free-fall motion is about 50–100 Hz, a relatively low-frequency signal with respect to those found by using traditional accelerometers. Because none of the traditional accelerometers possesses enough sensitivity in this frequency range, the force response of a free-fall motion can never be measured. As a micromachined process is compatible with a semiconductor process, a micromachine-based free-fall sensor designed using a PoD sensor is the only sensor at this time that allows us to meet our objective. In the next section, a micromachine-based PoD sensor will be implemented to experimentally demonstrate and verify this line of thought.

V. Experimental Setup

A 2000-μm-long by 20 μm-wide by 6–7-μm-thick micromachine-based PoD sensor designed by an APROPOS device is shown in Fig. 1(b), where the structure and geometry are also detailed. A 20.1-mm-long by 6-mm-wide by 1.8-mm-thick PZT plate with a uniform electrode was used as the reference signal, and the result is shown as the thick line in Fig. 2(a). The first resonant frequency of this PZT plate was 1.41 kHz. The corner wavenumber of the APROPOS device was set at 0.1, and its effective surface electrode was $R(x) = e^{-0.1|x|} - 0.5712\ \sin(0.01122x)$. The resonant frequency of this PoD sensor was set to 1.29 kHz. Substituting these parameters and values of the first resonant frequency into (4) that is the dispersion relationship, the corner frequency of the no-phase delay low-pass filter was found to be

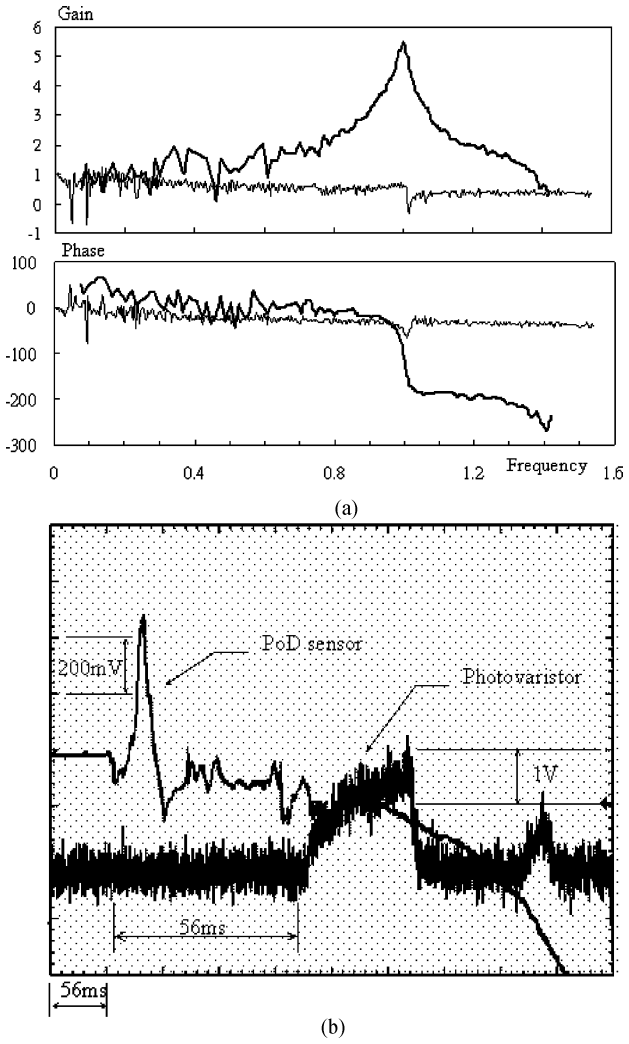

Fig. 2. (a) Normalized transfer function of 1) PZT plate (thick line) and 2) Micromachined-based PoD sensor (thin line). (b) Experimental results of a current-mode free-fall sensor designed as an APROPOS device concept within a PoD sensor design.

about 14.698 Hz and its transfer function

$$q_k(t) = z_k e_{31} w'''(x = o, t) \frac{1}{14.698 + \omega}. \tag{5}$$

The experimental results of this PoD sensor are shown as the thin line in Fig. 2(a). Both the gain and frequency of the PZT plate and PoD sensor were normalized so that comparisons would be possible. Note that the frequency response of the PoD sensor was flattened because of the effect of the APROPOS device and that no phase delay was associated with the gain tailoring. The experimental data also indicate that the usable bandwidth was enhanced to 95% of the first resonant frequency, which is about 1.2 kHz with the adoption of the APROPOS device.

To further verify the sensitivity and performance of the PoD sensor, a free-fall motion experiment identical with the setup previously used by Hsu and Lee [5] was performed, where a He–Ne laser light beam to a photovaristor was used to serve as a reference signal of the start of the free-fall motion. The implemented PoD sensor served as a free-fall sensor. A current amplifier with sensitivity of 10 V/nA coupled with a built-in electronic one-pole 10-kHz low-pass filter was used as the interface circuit, which was placed far from the first resonant

frequency of the PoD sensor to eliminate the high-frequency noise without influencing either the gain or the phase of the transfer function of the PoD sensor [Fig. 2(a)]. The digital oscilloscope was triggered by the photovaristor [5] and a 30% pretrigger was used to ensure that the time signal obtained would include the beginning of the fall. Note that the signal of the free fall was about 100 Hz, as mentioned previously [4], which was calculated from the time interval of the measured free-fall signal. The distance h between the He–Ne laser to the starting point of free-fall was about 1.7 cm, which corresponds to about 58.87 ms per the free-fall equation $h = gt^2/2$, where g equals the gravity constant 9.8 m/s^2. The time difference between this measured free fall to the photovaristor was about 56 ms, which is close to the predicted value of 58.87 ms. In summary, the experimental data obtained demonstrate very clearly that the performance of the micromachine-based miniature free-fall sensor can be designed and successfully implemented by adopting an APROPOS device concept in the design of a PoD sensor.

VI. Conclusion

The fundamental design view and principles related toward integrating an APROPOS device concept into PoD sensor design, that is, piezoelectric accelerometers and piezoelectric acceleration sensors, were presented. By taking advantage of the freedom of placing the targeted origin anywhere on the base structure of the sensor implemented by an APROPOS device, the vibration source can be measured directly without being delayed by the sensor structure itself when the targeted origin is placed at the fixed end. The performance of the PoD sensor developed by incorporating an APROPOS device demonstrates the development of a new class of accelerometers with a low first-resonant frequency and at the same time has a no-phase delay low-pass filter to reduce the gain of its first-resonant frequency and increase its low-frequency sensitivity without sacrificing bandwidth. Furthermore, adopting a micromachined process to implement this new class of accelerometer leads us to an optimum sensor for measuring free-fall motion. It can been seen that a miniature free-fall accelerometer measures free-fall motion without being affected by such factors as the detrimental noise generated by the sensor structure resonance, such as electronic filter-induced delay and distortion created by structure characteristics. In summary, experimental results prove that micromachine-based sensors and regular machine-based PoD sensors developed incorporating an APROPOS device concept are excellent innovative accelerometers for free-fall sensing.

Acknowledgment

The authors express their appreciation to Measurement Specialties, Sensor Products Division (MSI), for providing them with all the PVF2 films used in fabricating their piezoelectric devices.

References

[1] M. Serridge and T. R. Licht, *Piezoelectric Accelerometers and Vibration Preamplifiers, Theorie and Application Handbook,* Brüel & Kjær, Nærum, Denmark, 1986.

[2] A. Das and B. Wada, *Selected Papers on Smart Structures for Spacecraft*. Bellingham, WA: SPIE Optical Engineering Press, 2001.

[3] Y. H. Hsu and C. K. Lee, "Targeted origin placement for the autonomous gain-phase tailoring of piezoelectric sensors," *Smart Mater. Struct*., vol. 11, no. 3, pp. 444–458, Jun. 2002.

[4] Y. H. Hsu and C. K. Lee, "Miniature free-fall sensors," *J. Intelli. Mater. Syst. Struct*., vol. 12, no. 4, pp. 223–228, Apr. 2001.

[5] C. K. Lee, A. C. Munce, Jr., and T. C. O'Sullivan, "Disk drive with acceleration rate sensing," U.S. Patent 5 521 772, May 28, 1996.

[6] M. Madou, *Fundamentals of Micro Fabrication*. Boca Raton, FL: CRC Press, 1997.

Intersample Ripple-Free Multirate Control With Application to a Hard Disk Drive Servo

Qing-Wei Jia

***Abstract*—This paper discusses the intersample ripple problem in multirate control design. Supplementations and corrections have been made to the multirate control scheme proposed in [2]. Moreover, the proposed method is applied to a 5.25-in hard disk drive servo system. The experimental results show that the proposed method can handle the intersample ripples existing in the conventional design very well and that the new multirate control design demands a much smaller control input profile than the conventional design.**

***Index Terms*—Hard disk drive, multirate control system.**

I. Introduction

It is well known that in the digital control of continuous systems, the sampling rate is a critical design parameter. For better control performance, a faster sampling frequency relative to closed-loop bandwidth is desirable. However, computer and sensor constraints restrict the achievable sampling frequency. For example, in an embedded hard disk drive (HDD) servo system, the control system has to work with a limited sampling frequency because the position error signal (PES) measurement speed is limited to minimize the percentage of disk surface used for storing servo information, i.e., to maximize the data capacity.

With the fast development of microelectronics and digital signal-processing techniques, control system designers have long been resorting to multirate control techniques to deal with the problem of limited sampling frequency [1]–[17]. It has been shown that multirate-sampling technique may greatly improve the system performance, such as improving the transient system behavior, improving the system stability margins by relocating the plant zeros, enhancing the disturbance rejection property, etc. By changing the control input N times faster than the system output is sampled, Moore *et al*. [1] demonstrated that both the closed-loop poles and zeros can be arbitrarily assigned if the order of the controllers p and the input-updating coefficient N satisfy a certain condition. However, they also pointed out that the multirate strategy also produces a degradation in the intersample behavior, namely, intersample ripples may appear in the closed-loop system. This problem has also been pointed out by other researchers such as Goodwin and Feuer [3] and Tangirala *et al*. [4].

Intersample ripple is undesirable in industrial control applications because the plant output fluctuation may cause wear and tear on the actuator. A multirate control design was proposed in [5] to attack the intersample chattering. However, the method is only applicable to a control plant that has at least one integrator in its model, and it is required that the reference input of the system be a step signal. In [2], a new multirate control scheme for a general, linear time invariant system had been given based on the conventional multirate pole-zero assignment [1]. A constraint on the controller parameters was introduced in the new scheme to force the multirate control inputs to converge to a same constant level to eliminate the intersample ripple. In this paper, supplementations and corrections have been made to the multirate control scheme proposed in [2]. Moreover, the proposed method is applied to a 5.25-in HDD servo system. The experimental results show that

Manuscript received October 16, 2002; revised January 17, 2003, October 23, 2003, and August 10, 2004. Recommended by Technical Editor M. Tomizuka.

The author is with the Servo Department, Science Park Design Centre, Seagate Technology International, Singapore S118249 (e-mail: qwjia@ieee.org).

Digital Object Identifier 10.1109/TMECH.2005.848293